RSC Advances

Check for updates

An ultrasensitive isoprene gas sensor based on the In₂O₃/MoS₂ nanocomposite prepared by hydrothermal synthesis

Cheng Zhang,[ab] Jiuhong Wang,[ab] Ze Zhang,[ab] Jin Gong[ab] and Hairong Wang [ID] *[ab]

Isoprene is one of the specific biomarkers of liver disease in human exhaled gas, which should be detected with a high response at an order of ppb in actual application. In this paper, the heterojunction between n-type In₂O₃ and MoS₂ was proposed to improve the isoprene sensing properties. Both In₂O₃ and MoS₂ were prepared by a hydrothermal method, and nanostructured In₂O₃ flowers and solid micro irregular MoS₂ particles were mixed into the In₂O₃/MoS₂ composite with a mol ratio of 6 : 4. The composite was characterized by EDS and XRD to confirm the element types and crystal types. The isoprene sensor was prepared by dipping the composite suspension on a ceramic substrate integrated with a sensing electrode and heating unit. The testing results of the sensor showed the highest response value of 1.8 to 100 ppb isoprene at 200 °C. Besides, the low detecting limit (less than 5 ppb isoprene) and excellent selectivity are also revealed, showing that the composite can be a good candidate sensing material for isoprene for application in breath analysis.

Introduction

There are thousands of different components in human exhaled gases. The type and concentration of these gases depend on the body's internal metabolites and can reflect the health status of the body. For example, asthma can be diagnosed by detecting the exhaled low concentration NO gas.[1] Further study showed that the exhaled gases can be sensitive biomarkers of serious diseases. Kumar *et al.* compared the exhaled gases of patients with gastric/esophageal cancer and healthy volunteers, and found that the concentrations of exhaled VOCs (volatile organic compounds) like valeric acid, caproic acid, phenol, methyl phenol, ethyl phenol, butenal, valeric aldehyde, hexanal, heptanal, octanal, nonanal and isoprene in the cancer patients were significantly higher than those of the healthy body.[2] So far, many efforts have been paid to screening diagnosis of serious diseases at their early stage by detecting the concentrations of relative VOCs in the exhaled gases.

For the liver diseases, many researchers investigated the possibility of diagnosing them by the exhaled gases analysis. Vincentis *et al.* verified that some VOCs are specific respiratory markers for liver metabolic diseases.[3] Pijls *et al.* concluded that various types of VOCs of the human exhaled gases vary obviously in concentration during cirrhosis, which include alkenes, alkanes, alcohols and ketones.[4] Among the VOCs, isoprene is a typical one, which is sensitive and specific to abnormal

conditions of liver metabolism to a certain extent.[5] Research indicated that the concentration of isoprene in the human exhaled gas ranges from several ppb to hundreds of ppb. In order to detect the trace isoprene quickly, the gas sensors based on the metal oxide nanomaterial are often used for this purpose. Therefore, the nanostructured metal oxide gas sensors with high response, and very low detecting limitation to isoprene are needed badly in the breath analysis for liver diseases.

The metal oxide based gas sensors appeared in 1960s, and now they have been widely used in many applications.[6–8] The metal oxides have been thoroughly investigated such as SnO₂, TiO₂, In₂O₃, ZnO, and so on.[9–12] In₂O₃ as a typical n-type metal oxide with a wide band gap, and small resistivity, has high catalytic activity to VOCs. In addition, the nanostructured In₂O₃ exhibits good response characteristics to some gases even at low concentration. For example, the In₂O₃ nanosheets can be used to detect the ppb-level ethanol with high response, good selectivity and long time stability, which attributed to the large specific surface area and a large number of oxygen vacancies.[13] The work of Yanbai Shen showed that In₂O₃ nano-film has high response, fast response to the ppb-level NO₂.[14] In addition, to further improve response, heterojunction composite can be used by mixing the In₂O₃ with other metal oxides. For example, the In₂O₃ and ZnO composite has a high response to H₂S at room temperature consumption.[15] In recent years, more works studied different In₂O₃ nanomaterials,[16,17] and some of them tried to decrease low limit of detection of isoprene using In₂O₃. Testing results showed that nanostructured In₂O₃ is more suitable for the detection of ppb-level isoprene as being

compared with other metal oxide materials, and it has the advantages of higher conductivity and lower detecting limitation. The research showed high responses of the pure nanoflower In_2O_3 (ref. 18) or nanoflower In_2O_3 doped by Pt to isoprene.[19] Q. Zheng *et al.* found that the nanoparticle In_2O_3 sensor has a high response to isoprene and a very short response time, and can detect ppb-level isoprene. The significantly improved sensing performance of the In_2O_3 sensor for isoprene detection may be attributed mainly to a large number of oxygen vacancies generated during synthesis.[20] H. Jung *et al.* verified that Pd-coated In_2O_3 has excellent isoprene sensing performance due to the higher density of oxygen vacancies.[21] In order to have better isoprene detection characteristics, In_2O_3 can be combined with other metal oxides to form heterojunctions, such as the flower-like Cr_2O_3-doped In_2O_3 nanorods showing ultra-low detecting limitation to isoprene.[22] Moreover, the sensors based on $Au@Cr_2O_3–In_2O_3$ nanorods can detect isoprene at high humidity.[23]

When one attempts to develop a p–n heterojunction, MoS_2 is often used as a p-type semiconductor, which is widely used in gas sensors.[24] Nano-structured MoS_2 has high specific surface area and electron mobility, which is conducive to detect ultra-low concentration VOCs.[25] MoS_2 can be modified or doped with other metal oxide to form composite materials to further improve its performance as a gas sensing material.[26] Dongzhi Zhang *et al.* prepared p–n heterojunction nanocomposite of MoS_2 and In_2O_3 for formaldehyde detection. The In_2O_3 is nano-cube-shaped nanostructure, and the In_2O_3 nanocube contacts well with the flower-like MoS_2 microsphere. The testing results showed that the gas-sensitive properties of the In_2O_3/MoS_2 nanocomposite are better than those of the single In_2O_3 or MoS_2, and it has the characteristics of fast response, short recovery time and good repeatability. The improved response characteristics by a p–n heterojunction composite are mainly attributed to the stable depletion layers of the two materials caused by the energy band bending, the unique nanostructure, the high proportion of gas diffusion reachable sites and the special interaction between formaldehyde gas and the nanocomposite.[27] Furthermore, the presence of p–n heterostructure is also beneficial to improve the long-term stability of the material gas sensitive response.[28] In the breath diagnosis, extreme high response is expected to isoprene for the gas sensor, and the nanocomposite consisting of nanoflower In_2O_3 and nanoparticles MoS_2 is supposed to be a good candidate for the isoprene sensing. Theoretically, the two nanostructured materials have different work functions and band gaps, and the heterojunction formed in the composite may lead to energy band bending of the two materials, resulting in the more oxygen vacancies on the surface of the MoS_2. Therefore, the composite will obtain the enhanced responses, fast responses and low detecting limitation to isoprene. The combination of nanoflower In_2O_3 and nanoparticles MoS_2 has seldomly been reported before. In this paper, both nanoflower In_2O_3 and nanoparticle MoS_2 were prepared by hydrothermal method, and their composite as gas sensitive material to isoprene was studied. The response characteristics of the sensor were analyzed.

Experimental

Synthesis of the In_2O_3/MoS_2 composite

The In_2O_3/MoS_2 composite was prepared by hydrothermal method. First, we put 5 mmol ammonium molybdate, 30 mmol thiourea, and 5 mmol ammonium fluoride into 50 ml distilled water, and stir it vigorously in a magnetic mixer for 30 minutes, and then add 2 mmol citric acid. Then put the mixed solution into the 100 ml PTFE lined reactor, and then put the reactor into the constant temperature drying oven, and the temperature is set at 200 °C, heated for 24 h. Next, the obtained MoS_2 suspension was washed by anhydrous ethanol and deionized water for several times, followed by ultrasonic cleaning for 10 minutes, and then was centrifuged in a centrifuge at 4000 rpm for 30 minutes, and repeat the above cleaning step 3 times. The remaining suspension was dried in a thermostatic drying oven at 80 °C for 18 h to produce a black MoS_2 powder. Next, 0.6 mmol indium chloride and 3 mmol sodium hydroxide were added to 50 ml distilled water, respectively, and stirred in a magnetic mixer for 30 minutes. We put the mixed solution into 100 ml PTFE lined stainless steel reactor, and then put the reactor into a constant temperature drying oven. The temperature was set at 160 °C, heated for 18 h to get In_2O_3 suspension. Then the obtained 0.4 mmol MoS_2 in the first step was mixed with 0.3 mmol In_2O_3 and stirred by magnetic force for 6 h, and then put into a drying oven with a constant temperature of 190 °C for 24 h. The precipitation was washed by anhydrous ethanol and deionized water for several times, followed by ultrasonic cleaning for 10 minutes, and then was centrifuged in a centrifuge at 4000 rpm for 30 minutes, and repeat the above cleaning step 3 times. The remaining suspension was then dried in a thermostatic drying oven at 80 °C for 18 h to produce the black In_2O_3/MoS_2 powder. The preparation process is shown in Fig. 1.

Fabrication and measurement of the gas sensors

The prepared powder of the sensitive material was put into the test tube. A small amount of anhydrous ethanol was added, and the suspension of the sensitive material was prepared by ultrasonic for 10 minutes. And then, we selected a $3 \times 3 \times 0.25$ mm planar ceramic sheet, with two sensitive electrodes on the front side, and heating wire and two heating electrodes on the back side. The suspension were coated in the middle
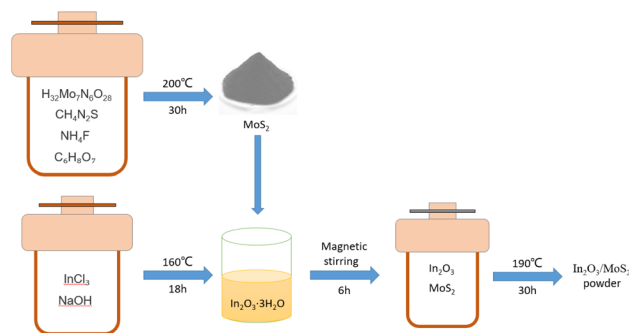

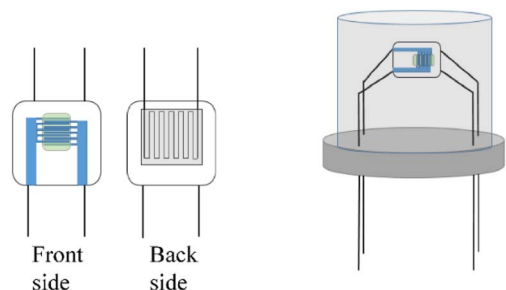**Fig. 1** Preparation of composite material process diagram.

Fig. 2 Flat ceramic sheet and TO package.

position of the ceramic sensitive electrode with a dropper, so that the originally disconnected sensitive electrode formed a closed loop through the sensitive material. The resistance change between the two sensitive electrodes was measured with a multimeter, and the voltage was applied to the two heating electrodes. The heating plate provided different temperatures to the sensor. Finally, the four pins of the ceramic sheet were welded to the sensor TO packaging base with soldering tin as shown in Fig. 2.

The gas distribution system used for testing is shown in Fig. 3. The mass flow meter was controlled by computer, and different percentages of isoprene and dry air were added respectively to configure different concentrations of isoprene. Marked resistance to stability of the sensor in the air as R_a, and then recorded the change of sensor resistance after inletting isoprene. Marked resistance to stability of the sensor in isoprene as R_g, and the response of the sensor was defined as eqn (1). The response time and recovery time were defined as the time required for the sensor to reach 90% of the total resistance changes in the case of adsorption or desorption, respectively. In the process of testing, the change of the resistance was tested and recorded by using the multimeter (Agilent 34970 A) with a computer real-time.

$$\text{Response} = R_a/R_g \tag{1}$$

When we tested isoprene, gas 1 was 100 ppb of isoprene with dry air as the background gas, and gas 2 was dry air. Different concentrations of isoprene can be prepared by controlling the percentage of the two gas channels with the mass flow meter.
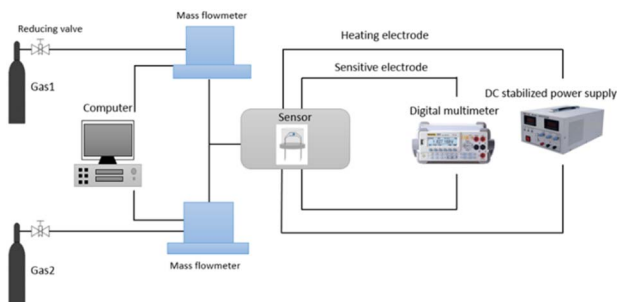
For example, 5 ppb isoprene can be prepared by 5% gas 1 (100 ppb isoprene) and 95% gas 2 (dry air). When we test other gases, gas 1 is a 5 ppm standard gas with dry air as the background gas, and gas 2 is dry air. For example, when we test formaldehyde selectivity, 2% gas 1 (5 ppm formaldehyde) and 98% gas 2 (dry air) can prepare 100 ppb formaldehyde. All tests are carried out in dry air.

Results

Characterization

As seen from Fig. 4, In_2O_3 is in the shape of flower nanospheres with a diameter of about 2 μm, and MoS_2 is in the shape of particle micro/nano structure with a size of about 2 μm. The final composite is about 100–200 nm nanoparticles with larger specific surface area, which is predetermined by the composite material. EDS shows the distribution of Mo and In elements, and it can be seen that the two materials are uniformly distributed on a whole, which can maintain the consistency of material preparation and the repeatability of gas sensitive response characteristics of the material.

XRD (X-ray diffraction) patterns of In_2O_3, MoS_2, and In_2O_3/MoS_2 composite were shown in Fig. 5 (using an instrument model D8 ADVANCE A25, Germany, rated voltage 60 kV, rated current 60 mA) using Cu Kα radiation (wavelength λ = 1.54056 Å), and the test range was 10°–80°. The diffraction angle is good. and compare with In_2O_3 standard card (JCPDS 71-2195), the angle of the main characteristic peaks are observed at 2θ of 21.253°, 30.631°, 35.518°, 45.683°, 51.039° and 60.691°, which correspond to the (211), (222), (400), (431), (440) and (622) planes respectively when it was compared with In_2O_3 standard card (JCPDS 71-2195). The material belongs to cubic crystal type iron manganese ore type, with grain size in 26–37 nm. The MoS_2 pattern was compared with the standard card (JCPDS 74-0932), showing that the angles of the main characteristic peaks are observed at 2θ of 13.659°, 32.903°, 37.879° and 57.111°, which correspond to (003), (101), (104), and (110) planes. The crystal
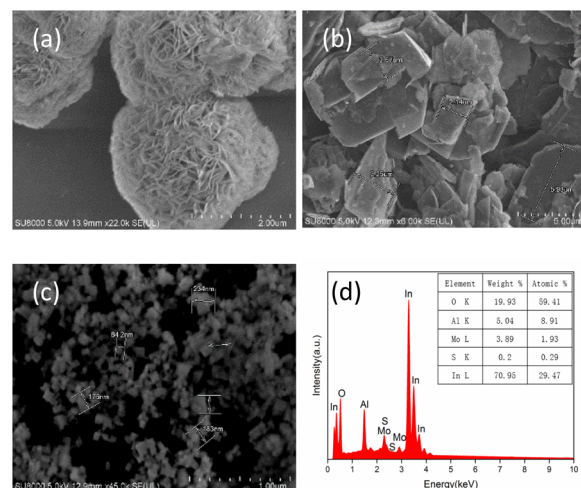

Fig. 3 The system for testing of the gas sensor.

Fig. 4 SEM images of (a) In_2O_3, (b) MoS_2 and (c) In_2O_3/MoS_2 composite. (d) EDS of In_2O_3/MoS_2 composite.
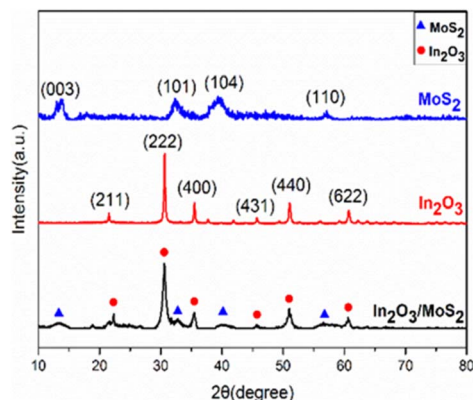
Fig. 5 XRD patterns of In_2O_3, MoS_2, and In_2O_3/MoS_2 composite.

Fig. 7 Real-time response resistance of the sensor.

type was tri-crystalline molybdenite type, and the grain size was in 12–21 nm.

Gas sensing characteristics

The optimal operating temperature of the sensor is an important gas sensing property, and then Fig. 6(a) describes the response curves of In_2O_3/MoS_2 sensor towards 100 ppb isoprene at operating temperature ranges from 150 to 250 °C. The response of the sensor increased at beginning and reached maximum response at the optimum operating temperature, and then it declined. So the optimal operating temperature of In_2O_3/MoS_2 sensor is 200 °C as shown in Fig. 6(b). The response of the sensor with different isoprene concentrations from 5 ppb
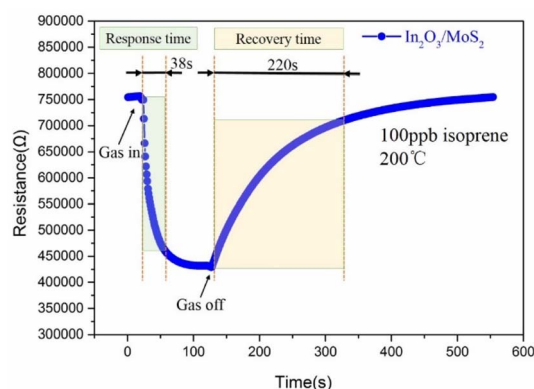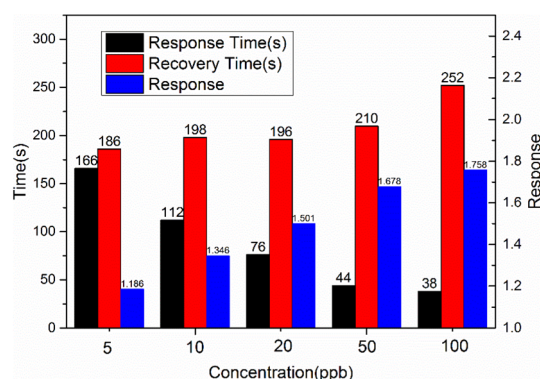

Fig. 8 Response, response time and recovery time of the sensor to different concentrations of isoprene.

to 100 ppb at the optimal operating temperature as shown in Fig. 6(c). The results show that the sensor has an obvious response to low concentration of isoprene, with a response value of 1.18 to 5 ppb isoprene while the pure In_2O_3 sensor get 1.10. The real-time response resistance of the sensor as shown in Fig. 7, and the results show that a short response time is 38 s of the sensor with a response value of 1.8 to 100 ppb isoprene. The response and recovery time and response of the sensor to different concentrations of isoprene is shown in Fig. 8. With the
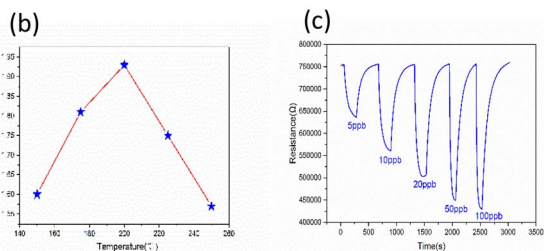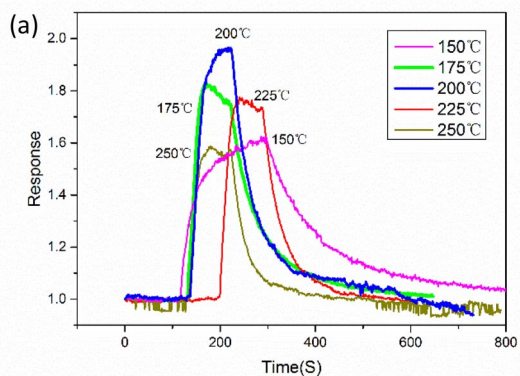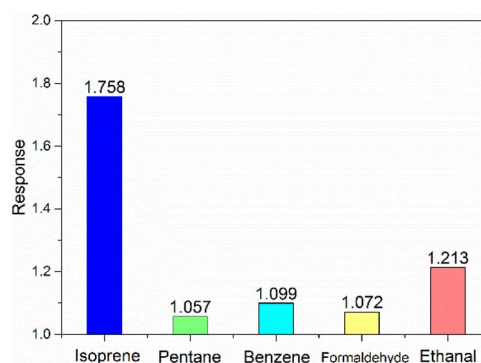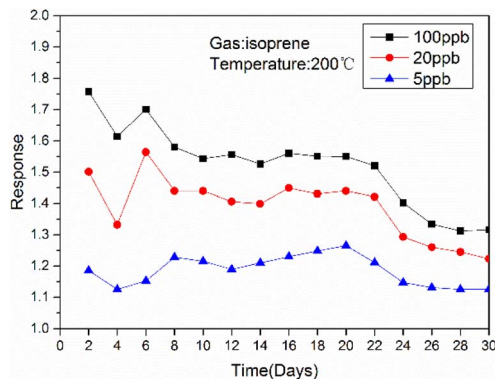

Fig. 6 (a) Response curves at different temperatures, (b) the optimum operating temperature of the sensor and (c) the response to different concentrations of isoprene.

Fig. 9 Selectivity of the sensor.

Fig. 10 The long-term stability of the sensor to different concentrations of isoprene at 200 °C.

Fig. 11 Gas sensing process.

increase of isoprene concentration, the recovery time and the response of the sensor increase, and the response time decreases, and the fastest response time is 38 s at 100 ppb isoprene. The response of the sensor to five gases at the same concentration (100 ppb) and same work temperature (200 °C) are shown in Fig. 9. The sensor is more sensitive to isoprene than other gases, so it has better selectivity. The long-term stability of the sensor to different concentrations of isoprene at 200 °C is shown in Fig. 10, and the response of the sensor decreased significantly after 20 days. As shown in Table 1, the response time of In_2O_3 NPs[20] is shortest, but the working temperature of this material is very high. Besides this material, the In_2O_3/MoS_2 sensor in this work has the fastest response speed. Pd-coated In_2O_3 (ref. 21) has minimum detection limit, but no specific response value, so in terms of test results, the In_2O_3/MoS_2 sensor in this work has the lowest detection limit.

Discussion

The isoprene gas sensor based on the In_2O_3/MoS_2 nanocomposite prepared by hydrothermal synthesis demonstrated excellent sensing properties, such as low detecting limitation (less than 5 ppb isoprene), and faster response (38 s of 100 ppb isoprene). Once materials are brought into the air, nanomaterials will adsorb oxygen in the air, and then react with isoprene. After electron gain and loss, a large number of free electrons will be generated, resulting in an increase in the electrical conductivity of the material and a decrease in the
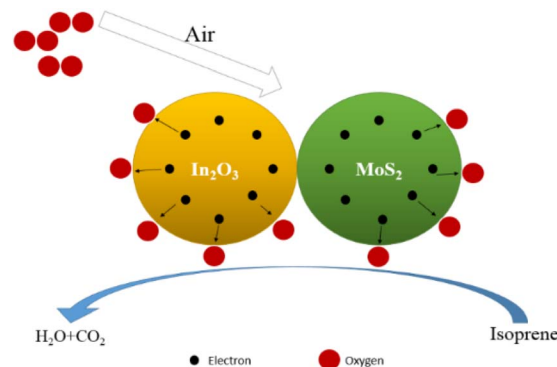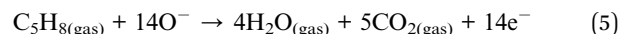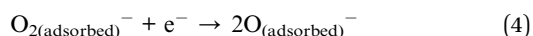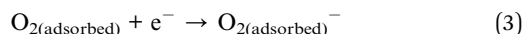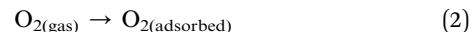
electrical resistance. The existence mode of oxygen is mostly as O^- with the temperature between 150 °C to 400 °C.[29] The specific reaction process is as eqn (2)–(5) and Fig. 11.

$$O_{2(gas)} \rightarrow O_{2(adsorbed)} \tag{2}$$

$$O_{2(adsorbed)} + e^- \rightarrow O_{2(adsorbed)}^- \tag{3}$$

$$O_{2(adsorbed)}^- + e^- \rightarrow 2O_{(adsorbed)}^- \tag{4}$$

$$C_5H_{8(gas)} + 14O^- \rightarrow 4H_2O_{(gas)} + 5CO_{2(gas)} + 14e^- \tag{5}$$

The composite material of In_2O_3 and MoS_2 has larger specific surface area, which enables the sensor to absorb more gas molecules when contacting isoprene, acquiring electrons more quickly and reducing resistance;[30] on the other hand, the work function and band gap of MoS_2 and In_2O_3 are $W_1 = 5.2$ eV, $E_{g1} = 1.9$ eV (ref. 31) and $W_2 = 4.3$ eV, $E_{g2} = 3.6$ eV, respectively.[32]

The band gaps of the two metal oxides are different, that leads to the band bending at the junction of the two materials,[33] and increases the electron migration rate.[34] Moreover, compared to a single metal oxide semiconductor material, two kinds of composite materials can form heterojunction, and when the sensor exposed to isoprene, the sensor can produce electronic depletion region faster, forming more oxygen vacancies or free electrons, as shown in Fig. 12. The electron can increase, electrons and holes recombination rate larger so as to overall improve the response of the sensor and the lower detection limit.

Table 1 Comparison of gas-sensing characteristics of isoprene sensors based on nanostructured In_2O_3

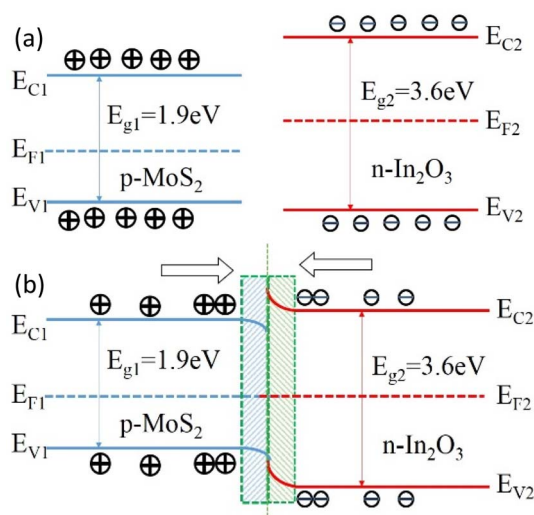| Sensing materials	Isoprene (ppb)	Response	Operation temperature (°C)	Response time (s)	Reference
Flower In_2O_3	500	3.1	190	53	18
Pt-decorated In_2O_3	1000	69.6	200	124	19
Cr_2O_3-doped In_2O_3	500	2.6	240	135	22
Au@Cr_2O_3–In_2O_3	1000	6.4	180	52	23
In_2O_3 NPs	1000	231	350	3	20
Pd-coated In_2O_3	0.4	—	196	100	21
In_2O_3/MoS_2	100	1.8	200	38	This work

Fig. 12 Energy band structure diagram of (a) p-type MoS_2, n-type In_2O_3 and (b) n-type In_2O_3/MoS_2 heterojunction.

Conclusions

The isoprene sensor based In_2O_3/MoS_2 composite was prepared by the dipping the composite suspension on a flat ceramic sheet, and the sensor was characterized and tested. Test results showed the sensor has low detection limit of less than 5 ppb and the fastest response time is 38 s at 100 ppb isoprene and higher responses to isoprene over other gases. In_2O_3/MoS_2 composite has a very low detection limit for isoprene gas, and has good response and selectivity. We can continue to study the application of this composite material for the feasibility of breath detection.

Conflicts of interest

There are no conflicts to declare.

Acknowledgements

References

1 R. Neelamegan, V. Saka, K. Tamilarasu, M. Rajaram, S. Selvarajan and A. Chandrasekaran, Clinical Utility of Fractional exhaled Nitric Oxide (FeNO) as a Biomarker to Predict Severity of Disease and Response to Inhaled Corticosteroid (ICS) in Asthma Patients, *J. Clin. Diagn. Res.*, 2016, **10**, Fc01–fc06.

2 S. Kumar, J. Huang, N. Abbassi-Ghadi, H. A. Mackenzie, K. A. Veselkov, J. M. Hoare, L. B. Lovat, P. Španěl, D. Smith and G. B. Hanna, Mass Spectrometric Analysis of Exhaled Breath for the Identification of Volatile Organic Compound Biomarkers in Esophageal and Gastric Adenocarinoma, *Ann. Surg.*, 2015, **262**, 981–990.

3 A. De Vincentis, U. Vespasiani-Gentilucci, A. Sabatini, R. Antonelli-Incalzi and A. Picardi, Exhaled breath analysis in hepatology: State-of-the-art and perspectives, *World J. Gastroenterol.*, 2019, **25**, 4043–4050.

4 K. E. Pijls, A. Smolinska, D. M. A. E. Jonkers, J. W. Dallinga, A. A. M. Masclee, G. H. Koek and F.-J. van Schooten, A profile of volatile organic compounds in exhaled air as a potential non-invasive biomarker for liver cirrhosis, *Sci. Rep.*, 2016, **6**, 19903.

5 K. Eng, N. Alkhouri, F. Cikach, N. Patel, C. Yan, D. Grove, R. Lopez, E. Rome and R. A. Dweik, Analysis of breath volatile organic compounds in children with chronic liver disease compared to healthy controls, *J. Breath Res.*, 2015, **9**, 026002.

6 T. Simon, N. Barsan, M. Bauer and U. Weimar, Micromachined metal oxide gas sensors: opportunities to improve sensor performance, *Sens. Actuators, B*, 2001, **73**, 1–26.

7 N. Barsan, D. Koziej and U. Weimar, Metal oxide-based gas sensor research: How to, *Sens. Actuators, B*, 2007, **121**, 18–35.

8 J. Janata, *Principles of Chemical Sensors*, 2009.

9 Q. Zhao, Y. Xie, T. Dong and Z. Zhang, Oxidation−Crystallization Process of Colloids: An Effective Approach for the Morphology Controllable Synthesis of SnO_2 Hollow Spheres and Rod Bundles, *J. Phys. Chem. C*, 2007, **111**, 11598–11603.

10 R. Dolbec and M. A. El Khakani, Sub-ppm sensitivity towards carbon monoxide by means of pulsed laser deposited SnO_2: Pt based sensors, *Appl. Phys. Lett.*, 2007, **90**, 173114.

11 K. D. Kim, S. H. Kim and H. T. Kim, Applying the Taguchi method to the optimization for the synthesis of TiO_2 nanoparticles by hydrolysis of TEOT in micelles, *Colloids Surf., A*, 2005, **254**, 99–105.

12 M. Liu, Z. Cheng, J. Yan, L. Qiang, X. Ru, F. Liu, D. Ding and J. Li, Preparation and Characterization of TiO_2 Nanofibers via Using Polylactic Acid as Template, *J. Appl. Polym. Sci.*, 2013, **128**, 1095–1100.

13 J. Liu, X. Lin, M. Sun, B. Du, L. Li, J. Bai and M. Zhou, Thiourea-assistant growth of In_2O_3 porous pompon assembled from 2D nanosheets for enhanced ethanol sensing performance, *Talanta*, 2020, **219**, 121323.

14 Y. Shen, X. Zhong, J. Zhang, T. Li, S. Zhao, B. Cui, D. Wei, Y. Zhang and K. Wei, In-situ growth of mesoporous In_2O_3 nanorod arrays on a porous ceramic substrate for ppb-level NO_2 detection at room temperature, *Appl. Surf. Sci.*, 2019, **498**, 143873.

15 M. Sun, H. Yu, X.-t. Dong, L. Xia and Y. Yang, Sedum lineare flower-like ordered mesoporous In_2O_3/ZnO gas sensing materials with high sensitive response to H_2S at room temperature prepared by self-assembled of 2D nanosheets, *J. Alloys Compd.*, 2020, **844**, 156170.

16 Z. Li, H. Yan, S. Yuan, Y. Fan and J. Zhan, In_2O_3 microbundles constructed with well-aligned single-

crystalline nanorods: F127-directed self-assembly and enhanced gas sensing performance, *J. Colloid Interface Sci.*, 2011, **354**, 89–93.

17 H. Dong, Y. Liu, G. Li, X. Wang, D. Xu, Z. Chen, T. Zhang, J. Wang and L. Zhang, Hierarchically rosette-like In$_2$O$_3$ microspheres for volatile organic compounds gas sensors, *Sens. Actuators, B*, 2013, **178**, 302–309.

18 B. Han, J. Wang, W. Yang, X. Chena, H. Wang, J. Chen, C. Zhang, J. Sun and X. Wei, Hydrothermal synthesis of flower-like In$_2$O$_3$ as a chemiresistive isoprene sensor for breath analysis, *Sens. Actuators, B*, 2020, **309**, 127788.

19 B. Han, H. Wang, W. Yang, J. Wang and X. Wei, Hierarchical Pt-decorated In$_2$O$_3$ microspheres with highly enhanced isoprene sensing properties, *Ceram. Int.*, 2021, **47**, 9477–9485.

20 Q. Zheng, J. H. Lee, S.-J. Kim, H.-S. Lee and W. Lee, Excellent isoprene-sensing performance of In$_2$O$_3$ nanoparticles for breath analyzer applications, *Sens. Actuators, B*, 2021, **327**, 128892.

21 H. Jung, H. Min, J. Hwang, J. Kim, Y.-S. Choe, H.-S. Lee and W. Lee, Selective detection of sub-1-ppb level isoprene using Pd-coated In$_2$O$_3$ thin film integrated in portable gas chromatography, *Appl. Surf. Sci.*, 2022, **586**, 152827.

22 X. Wu, H. Wang, J. Wang, J. Chen, L. Shi, B. Han and X. Tian, Hydrothermal synthesis of flower-like Cr$_2$O$_3$-doped In$_2$O$_3$ nanorods clusters for ultra-low isoprene detection, *Colloids Surf., A*, 2021, **620**, 126606.

23 X. Wu, H. Wang, J. Wang, D. Wang, L. Shi, X. Tian and J. Sun, VOCs gas sensor based on MOFs derived porous Au@Cr$_2$O$_3$-In$_2$O$_3$ nanorods for breath analysis, *Colloids Surf., A*, 2022, **632**, 127752.

24 A. Shokri and N. Salami, Gas sensor based on MoS$_2$ monolayer, *Sens. Actuators, B*, 2016, **236**, 378–385.

25 M. Donarelli, S. Prezioso, F. Perrozzi, F. Bisti, M. Nardone, L. Giancaterini, C. Cantalini and L. Ottaviano, Response to NO$_2$ and other gases of resistive chemically exfoliated MoS$_2$-based gas sensors, *Sens. Actuators, B*, 2015, **207**, 602–613.

26 Y. Zhang, W. Zeng and Y. Li, The hydrothermal synthesis of 3D hierarchical porous MoS$_2$ microspheres assembled by nanosheets with excellent gas sensing properties, *J. Alloys Compd.*, 2018, **749**, 355–362.

27 D. Zhang, C. Jiang and J. Wu, Layer-by-layer assembled In$_2$O$_3$ nanocubes/flower-like MoS$_2$ nanofilm for room temperature formaldehyde sensing, *Sens. Actuators, B*, 2018, **273**, 176–184.

28 X. Li, N. Zhang, C. Liu, S. Adimi, J. Zhou, D. Liu and S. Ruan, Enhanced gas sensing properties for formaldehyde based on ZnO/Zn$_2$SnO$_4$ composites from one-step hydrothermal synthesis, *J. Alloys Compd.*, 2021, **850**, 156606.

29 A. Mirzaei, S. G. Leonardi and G. Neri, Detection of hazardous volatile organic compounds (VOCs) by metal oxide nanostructures-based gas sensors: A review, *Ceram. Int.*, 2016, **42**, 15119–15141.

30 J. Liu, S. Li, B. Zhang, Y. Wang, Y. Gao, X. Liang, Y. Wang and G. Lu, Flower-like In$_2$O$_3$ modified by reduced graphene oxide sheets serving as a highly sensitive gas sensor for trace NO$_2$ detection, *J. Colloid Interface Sci.*, 2017, **504**, 206–213.

31 Y. Liu, S. Li, S. Xiao and K. Du, Down to ppb level NO$_2$ detection by vertically MoS$_2$ nanoflakes grown on In$_2$O$_3$ microtubes at room temperature, *Colloids Surf., A*, 2022, **648**, 129435.

32 Z. Yang, D. Zhang and H. Chen, MOF-derived indium oxide hollow microtubes/MoS$_2$ nanoparticles for NO$_2$ gas sensing, *Sens. Actuators, B*, 2019, **300**, 127037.

33 J. Mu, B. Chen, M. Zhang, Z. Guo, P. Zhang, Z. Zhang, Y. Sun, C. Shao and Y. Liu, Enhancement of the Visible-Light Photocatalytic Activity of In$_2$O$_3$-TiO$_2$ Nanofiber Heteroarchitectures, *ACS Appl. Mater. Interfaces*, 2012, **4**, 424–430.

34 D. Zhang, Y. Sun, C. Jiang and Y. Zhang, Room temperature hydrogen gas sensor based on palladium decorated tin oxide/molybdenum disulfide ternary hybrid via hydrothermal route, *Sens. Actuators, B*, 2017, **242**, 15–24.